Fusion of Radar, LiDAR and Thermal Information for Hazard Detection in Low Visibility Environments

Paul Fritsche, Björn Zeise, Patrick Hemme and Bernardo Wagner
Institute of Systems Engineering - Real Time Systems Group
Leibniz Universität Hannover, Appelstr. 9A, D-30167 Hannover, Germany
fritsche | zeise | hemme | wagner @rts.uni-hannover.de

***Abstract*— Nowadays, mobile robots are widely used to support fire brigades in search and rescue missions. The utilization of those robots – especially under low visibility conditions due to smoke, fog or dust – is limited. Under these circumstances, environmental perception is still a huge challenge. In this work, we present an approach on using LiDAR, radar, and thermal imaging in order to detect hazards that are potentially harmful to the robot or firefighters. We show the benefits of fusing LiDAR and radar before projecting temperatures recorded with a thermal imaging camera onto the range scans. Additionally, a hotspot detection method using the tempered range scans is presented. We demonstrate the functionality of our approach by teleoperating a robot through a smoky room.**

I. Introduction

The exploration of disaster environments with severely restricted visibility is dangerous for first responders as they have no knowledge of the current situation and can lose their orientation in the unknown environment. In such dangerous scenarios, a mobile robot can form an overall perspective on the situation and deliver useful information to first responders [1].

Depending on the environment and application, an operator can equip a robot with suitable sensors to detect hazards. An example is given in [2], where the authors used a radiation and a chemical sensor to sense and localize sources of hazards. Optical sensors such as laser scanners and RGB cameras are commonly used for most tasks in mobile robotics and have established themselves as state-of-the-art, but they are severely limited in low visibility environments as shown in Figure 1.

Sensors such as radar scanners and thermal imaging cameras (TICs) can overcome poor visibility conditions but have other limitations in their physical properties. Radar sensors are unable to represent the structure of an environment in the same quality as a LiDAR due to limited range and angular resolution. The temperatures measured by a TIC depend on the material of an object. Additionally, the images can contain reflections which lead to a misinterpretation [3].

Nevertheless, connecting thermal images with structural information brings benefits to the exploration of hazardous environments. One application concept is shown in [4], where distance information from a radar is projected on an infrared image integrated on a small head-mounted display to indicate free space for firefighters. Schoenauer et al. [5] developed a mobile sensor system worn by firemen to construct thermal maps with a depth sensor and a TIC.

Fig. 1: Robot in low visibility environment

In this work, we present a new approach to detecting hazards with a mobile robot in low visibility environments. Therefore, we fuse range data from a LiDAR and a radar sensor to map the unknown environment and merge the fused range data with thermal information. Using the threefold sensor fusion, we realize hazard detection and visual hazard feature representation for first responders.

Initial investigations regarding radar sensors in the field of mobile robots were done at the Australian Centre for Field Robotics in the nineties, where fundamental probabilistic SLAM algorithms in combination with radar were developed [6]. In [7], Adams et al. used radar in the context of robotics for mapping of mines by utilizing a Probability Hypothesis Density (PHD) filter. In opposite to feature-based SLAM approaches, Vivet et al. [8] developed a scan matching method through a Fourier-Mellin transform producing large scale maps. Mapping of indoor environments was performed by Detlefsen [9] and Marck [4].

Research towards extrinsic calibration of a LiDAR and a camera was done in several works. One description of the extrinsic calibration of an RGB camera and a 2D LiDAR is given in [10]. A planar checkerboard pattern is used to find initial guesses for intrinsic and extrinsic parameters. After that, the calibration result is further refined using nonlinear minimization. In works such as [11] and [12], a similar procedure regarding the calibration between a 3D LiDAR and an RGB camera is described. In these approaches, planes are detected in both the laser and camera observations to determine the transformation between the sensor frames. Temperature mapping is a well-known problem not only in the robotics domain. Commonly, a ray tracing algorithm is

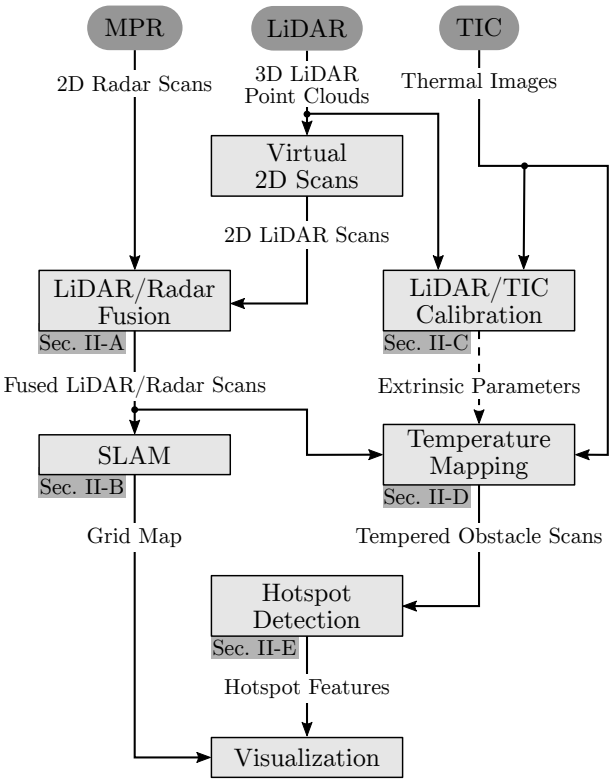

Fig. 2: Overview of the methods presented in this work.

implemented, that calculates the intersections of the laser rays and the camera's image plane. This principle has been applied by e.g. [13], [14] and [15] with different kinds of range sensors.

The remainder of this paper is organized as follows: In Section II, we describe methods improving robot perception in low visibility environments. This includes explanations on LiDAR/radar fusion and SLAM, temperature mapping using fused LiDAR/radar data and thermal images as well as hotspot detection. The evaluation presented in Section III demonstrates the benefits of our approach in low visibility scenarios. In Section IV, we conclude our work and give a short outlook.

II. Methods

In Figure 2, we illustrate the connection of all components contributing to our approach. At first, we fuse radar and LiDAR data to generate 2D obstacle scans that allow environmental perception and map generation under low visibility conditions. After that, we create a tempered obstacle scan by projecting temperature values onto the fused obstacle scan. Therefore, we need to run an extrinsic calibration between LiDAR and TIC after mounting all sensors onto the robot. Using the tempered obstacle scans and the position information of the robot obtained by our SLAM, we visualize hot spots in a user-friendly manner with a 2D map.

A. Fusing LiDAR, Radar and Thermal Information

We fuse a *Velodyne VLP-16* and the *Mechanical Pivoting Radar* (MPR), which was built by the Fraunhofer Institute

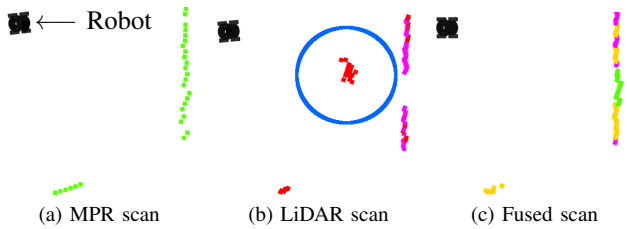

(a) MPR scan (b) LiDAR scan (c) Fused scan

Fig. 3: Our sensor fusion replaces LiDAR points, which are affected by smoke (blue circle), with radar points (green). Yellow points represent R_{Fusion}. Red and magenta points are LiDAR scan points. Magenta represents a line segmentation.

for High Frequency Physics and Radar Techniques for the SmokeBot[1] project. We presented the sensor and first results in [16]. The sensor fusion combines virtual 2D scans [17] with 2D radar scans to generate two fused 2D scans, one for SLAM and the other one for obstacle avoidance. We presented our sensorfusion and SLAM approach in [18]. In this paper, we present an evaluation of the composition of the fused scan S_{Fusion} during the presence of fog. A fused scan S_{Fusion} contains radar, LiDAR and fused scan points.

$$S_{\text{Fusion}} = [R_{\text{LiDAR}}, R_{\text{Radar}}, R_{\text{Fusion}}, Inf, ...] \quad (1)$$

The more aerosols, which disturb the LiDAR, an environment contains, the more radar scan points are in the fused scan S_{Fusion}.

Figure 3 shows results from first experiments, where we created low visibility conditions with a fog machine [16]. We observed two effects related to aerosols using the LiDAR. First, aerosols can lead to a detection, which is visualized with a blue circle in Figure 3b. We call this effect *Type I*.

If the LiDAR is very close or inside an aerosol cloud, then the laser pulses get absorbed and no interpretable echoes are received. Therefore, the sensor is interpreting it as an infinite measurement (Inf). We call this effect *Type II*.

There are several techniques for SLAM. Mainly, they can be divided into filter-based and optimization-based approaches. We presented a more detailed description of our SLAM approach in [18]. Our SLAM is based on ICP registration between the fused scan S_{Fusion} and a grid map. The data association is based on Euclidean distances and the distinction according to the fusion cases.

Additionally, our data association takes into account if a grid cell has been observed from the current robot position before by distinguishing eight viewing angles for every cell. Hence, we store in each cell the direction from where it has been seen.

After data association, we calculate the transformation between the fused scan and the grid map, which represents the measurement inside a Kalman filter. The prediction of the Kalman filter can be based on the odometry and the motion model of the robot or a linear motion model if no odometry is available.

[1] http://www.smokebot.eu/

The hotspot detection method presented in Section II-C relies on a robust temperature mapping approach. During temperature mapping, thermal images recorded by the TIC are projected onto range scan points. Those range scans can be pure LiDAR, pure radar or a combination of both. Since no explicit calibration between the radar scanner and the TIC is performed in this work, we assume the scans (regardless of their origin) to be provided with respect to the LiDAR coordinate frame. In order to calibrate the LiDAR and the TIC, we use a method that we presented in one of our previous works [19]. It is based on minimization of point-to-plane distances as described in [10].

B. 2D Tempered Obstacle Scans

A homogeneous, fused LiDAR/radar point ${}_{(L)}\tilde{\boldsymbol{x}}_{LR} = ({}_{(L)}\tilde{x}_{LR}, {}_{(L)}\tilde{y}_{LR}, {}_{(L)}\tilde{z}_{LR}, 1)^T$ with respect to $\boldsymbol{L}$, which is part of a fused scan S_{Fusion}, can be projected onto the TIC's image plane using the following expression:

$$\tilde{w} \begin{pmatrix} u \\ v \\ 1 \end{pmatrix} = \boldsymbol{K} \left[\boldsymbol{R}_{(LC)} \,|\, \boldsymbol{t}_{(LC)} \right] {}_{(L)}\tilde{\boldsymbol{x}}_{LR}, \tag{2}$$

with the priorly known intrinsic camera matrix $\boldsymbol{K}$, image coordinates $(u, v)^T$, scaling factor $\tilde{w}$ and extrinsic transformation matrix $\left[\boldsymbol{R}_{(LC)} \,|\, \boldsymbol{t}_{(LC)} \right]$. Since Equation 2 depicts a complete 3D-to-2D projection, the projection of a 2D fused LiDAR/radar point, i.e. a 3D point with a constant height ${}_{(L)}z_{LR}$, is straightforward. By assigning a temperature value to every individual point, a tempered obstacle scan S_{Temp} is being constructed.

When generating 2D fused LiDAR/radar scans S_{Fusion}, all obstacles relevant to the robot are taken into account. The same behavior is pursued during temperature mapping of a point ${}_{(L)}\boldsymbol{x}_{LR} = ({}_{(L)}x_{LR}, {}_{(L)}y_{LR}, {}_{(L)}z_{LR})^T$: Using the robot's dimensions, minimum and maximum heights z_{min} and z_{max}, respectively, are determined (see also Figure 4). With the help of those limits, two additional 3D points using z_{min} and z_{max} instead of ${}_{(L)}z_{LR}$ are projected onto the TIC's image plane. Along the vertical line between the resulting points ${}_{(I)}\boldsymbol{x}_{LR,\text{min}}$ and ${}_{(I)}\boldsymbol{x}_{LR,\text{max}}$, all corresponding temperatures in the thermal images are investigated. Only the highest temperature is integrated into the tempered obstacle scan.

C. Hotspot Detection

The tempered obstacle scans obtained from temperature mapping are used to detect hotspots. For this purpose, the scan points are clustered according to their temperatures. If a cluster reaches a predefined size and consists of points with temperatures greater than a specific threshold, we generate a hotspot feature. Besides the recording time stamp and the coordinate frame to which the hotspot's location is related, a hotspot feature contains the following information:

- Hotspot's location
- Variance of location
- Average temperature of all points belonging to the hotspot
- Variance of average temperature
- Size of hotspot cluster (number of points forming the hotspot)

Algorithm 1: Hotspot detection

Input : $S_{\text{Temp}} = \{\boldsymbol{x}_{\text{Temp}}^{(k)}\}$ with $k \in \{1, 2, ..., K\}$
T_{max}
Output: Array $\boldsymbol{h}$ containing hotspot features $h^{(l)}$ with $l \in \{1, 2, ..., L\}$

```
for k ← 1 to K do
    H ← InitializePointCloud()
    if T^(k) > T_max then
        Add x_Temp^(k) to H
    end
end
C ← EuclideanClusterExtraction(H)
L ← sizeof(C)
h ← InitializeArray()
for l ← 1 to L do
    x̄_Temp^(l) ← CalcMeans(C^(l))
    Var(C^(l)) ← CalcVars(C^(l), x̄_Temp^(l))
    NPnts ← sizeof(C^(l))
    h^(l) ← HotspotGen(x̄_Temp^(l), Var(C^(l)), NPnts)
    Add h^(l) to h
end
```

Algorithm 1 presents the hotspot detection procedure using a tempered obstacle scan S_{Temp} as input. A scan contains K tempered scan points $\boldsymbol{x}_{\text{Temp}}^{(k)} = \left(x^{(k)}, y^{(k)}, z^{(k)}, T^{(k)}\right)^T$. Every individual point is defined by 3D point coordinates ($x^{(k)}$, $y^{(k)}$ and $z^{(k)}$) as well as a temperature value $T^{(k)}$. Additionally, a temperature threshold T_{max} has to be provided. The result of this procedure is a vector $\boldsymbol{h}$ containing all detected hotspots including their properties mentioned above.

III. Evaluation

The following sections describe the experimental setup that was used to evaluate the presented methods. The focus was on the evaluation of the benefits of LiDAR/radar scan fusion and hotspot detection.

A. Experimental Setup

Figure 5 depicts the mobile robot platform (*taurob tracker*) that was used for evaluation. Besides several other sensors, the robot is equipped with a 3D LiDAR sensor, a 2D radar scanner and a thermal imaging camera.

The LiDAR used in the experiments is a *Velodyne VLP-16*. It provides 360° scans consisting of 16 horizontal scan lines. It is able to take measurements of up to 100 m and works at a rate of 10 Hz. The 2D radar scanner is the *MPR*, which provides range measurements at a maximum rate of 2.5 Hz. The measurement range is between 0.2 m and 15 m. The TIC in our experimental setup is a *FLIR A655sc* with a spatial

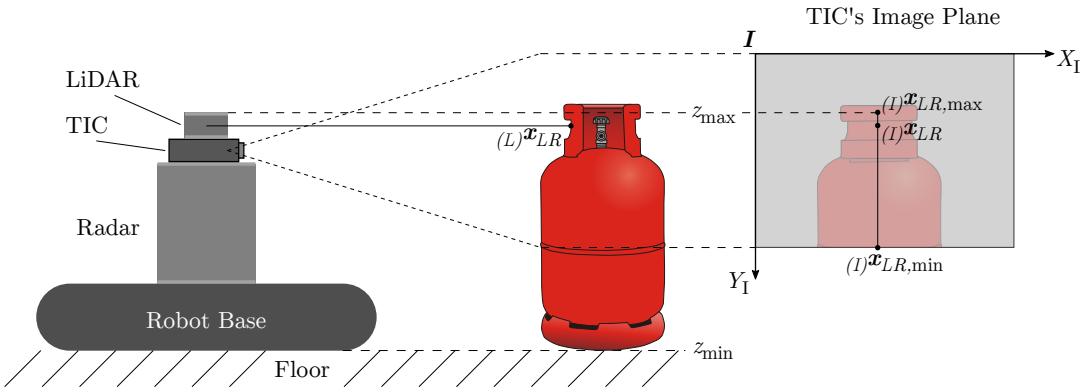

Fig. 4: Side view illustration of the robot platform and the sensor stack looking at a potential heat source: Using the robot's dimensions and corresponding vertical limits z_{min} and z_{max}, an imaginary line along those boundary points can be created in the thermal image (depicted on the right-hand side). Investigating all temperatures on the line between $_{(I)}\boldsymbol{x}_{LR,\text{min}}$ and $_{(I)}\boldsymbol{x}_{LR,\text{max}}$, only the highest one is integrated into the tempered obstacle scan S_{Temp}. If the projected pendants of z_{min} and z_{max} lie outside of the image, the limits are accordingly adapted (as is the case with $_{(I)}\boldsymbol{x}_{LR,\text{min}}$).

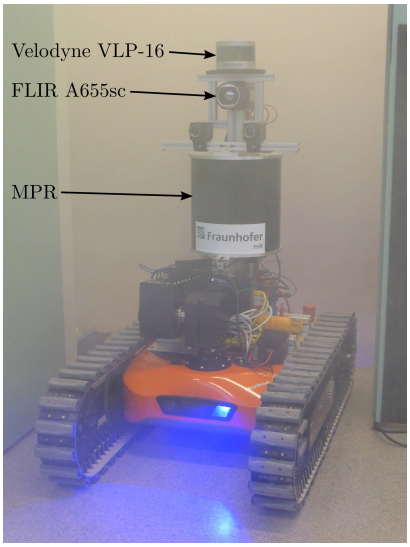

Fig. 5: Sensor setup

Fig. 6: Workshop environment with fog machine (left) and heat targets (marked with the green circles).

resolution of 640×480 pixels. It works in the spectral range between $7.5\,\mu\text{m}$ and $14\,\mu\text{m}$. The camera's FOV is $45° \times 34°$.

During our experiments, the robot was teleoperated inside a smoky workshop environment. In order to generate smoke, we used a fog machine. Although smoke and fog are physically different, their attenuating influence on light-based range measurement and vision is basically the same. For this reason, instead of creating real smoke, we only use dense fog in our experiments. For evaluating the benefits of the hotspot detection, we placed some electrically heated targets in the workshop (see Figure 6). After entering the smoky room, the robot was driven in circles around a metal cupboard a couple of times.

B. Scan Fusion

The sensor fusion between LiDAR and MPR provides two scans. One scan is used for SLAM in order to build a map. In combination with the virtual 2D scan method, our sensor fusion creates scans which contain as less as possible pure radar points (see Figure 7b) due to the integration of 3D LiDAR data. Only if no suitable LiDAR points are available, then radar is used at this certain area of the scan. We demonstrate a case without suitable LiDAR measurements in [18], where we drove into a small room that was completely filled with fog leaving only MPR scan points in S_{Fusion}. The near field scan of the sensor fusion is used for obstacle avoidance and hazard detection. As can be seen in Figure 9b, LiDAR scans can contain detected fog, which would lead to wrong obstacle and hazard detection. In this case, effect *Type I* occurs in the near scan field and our sensor fusion replaces the LiDAR points with radar points. Consequently, the compositions of the scans for hazard detection during the test run contain more radar points, as it can be seen in Figure 7a. The amount of fused scan points (weighted averaging) depends on how many objects can be seen by LiDAR and radar (e. g. yellow points in Figure 3c).

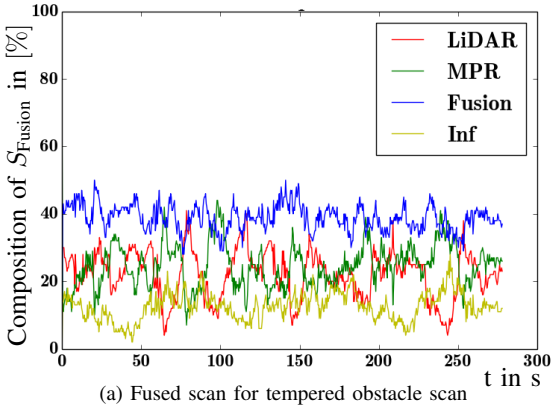

(a) Fused scan for tempered obstacle scan

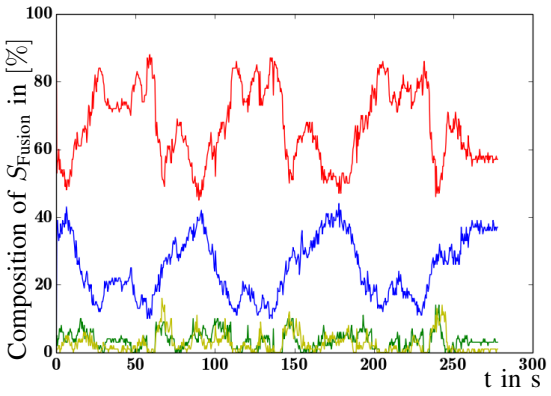

(b) Fused scan for SLAM

Fig. 7: Composition of the fused scans for SLAM and hazard detection during the experiment.

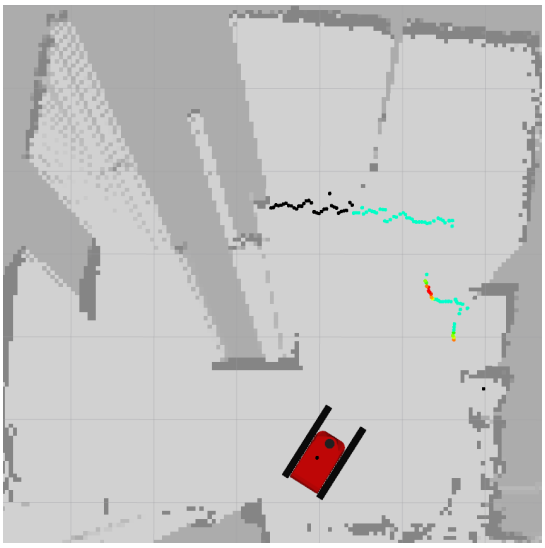

(a) Map with tempered obstacle scan

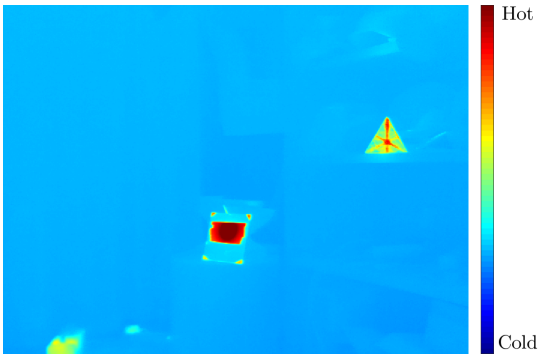

(b) Corresponding thermal image

Fig. 8: Top-down view of the workshop environment: (a) Several artificial hotspots have been placed in the room in order to show the functionality of the tempered obstacle scans, which are integrated into the 2D grid map generated using SLAM; (b) corresponding thermal image from the robot's point of view.

C. Hotspot Detection

Figure 8 shows the functionality of the map creation using our SLAM as well as the generation of tempered obstacle scans using fused LiDAR/radar scans and thermal images as input (see Section II-B). Comparing Figures 8a and 8b, it can be seen that the method for filtering the maximum temperatures from the thermal images before integrating them into the tempered obstacle scans works well: Both heat targets displayed in the thermal image can also be found in the tempered obstacle scan.

Since the room was filled with smoke during our experiment, the pure laser scans contain scattered points in the space between the robot and the actual obstacles. Comparing Figures 9a and 9b, the benefit of using fused LiDAR/radar scans for hotspot detection becomes clear: If the hotspot detection would have been performed on the pure laser scans (as depicted in Figure 9b), wrong hotspot features would be generated. In Figure 9a, where we used the fused LiDAR/radar scans during temperature mapping, the hotspot detection works well.

IV. Conclusion and Future Work

In this work, we presented methods improving mobile robot perception in smoky environments. We fused both laser and radar scans exploiting the individual sensors' advantages under different visibility conditions. The fused LiDAR/radar scans serve as input for a SLAM procedure that is able to generate a grid map representation of the environment. Additionally, we created tempered obstacle scans using fused LiDAR/radar data in combination with thermal images. With the help of those tempered scans, we were able to detect hotspot hazards.

During evaluation, we teleoperated a robot equipped with aforementioned sensors through a smoky workshop environment. We demonstrated that – by using fused LiDAR/radar information – on the one hand a robust grid map can be generated, and on the other hand hotspots can reliably be detected. The comparison between the hotspot detection

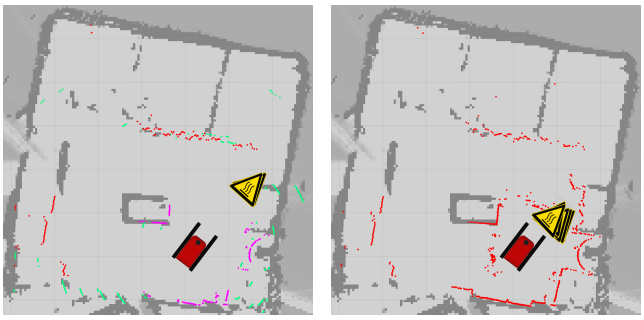

(a) Correctly detected hotspot (b) Wrongly detected hotspot

(c) Corresponding thermal image

Fig. 9: Top-down view of the workshop environment: (a) 2D grid map with fused LiDAR/radar scan and correctly detected hotspot; (b) wrongly detected hotspot due to usage of pure laser scans as input of temperature mapping; (c) corresponding thermal image from the robot's point of view.

relying on fused data and an approach using pure laser scan data as input showed obvious advantages on the side of the former one.

Future work will focus on the integration of the detected hotspot features into a specific map layer of the environmental representation. This will be done in a probabilistic way in order to cope with measurement uncertainties and corresponding misdetections.

ACKNOWLEDGMENT

This work has partly been supported within H2020-ICT by the European Commission under grant agreement number 645101 (SmokeBot).

REFERENCES

[1] R. R. Murphy, "Trial by fire [rescue robots]," *IEEE Robot. Automat. Mag.*, vol. 11, no. 3, pp. 50–61, 2004.

[2] C. W. Neilsen, D. I. Gertman, D. J. Bruemmer, R. S. Hartley, and M. C. Walton, "Evaluating robot technologies as tools to explore radiological and other hazardous environments," in *Proc. American Nuclear Society Emergency Planning and Response, and Robotics and Security Systems Joint Topical Meeting*, 2008.

[3] B. Zeise, S. P. Kleinschmidt, and B. Wagner, "Improving the interpretation of thermal images with the aid of emissivity's angular dependency," in *Proc. 2015 IEEE Int. Symp. Safety, Security, and Rescue Robotics*. IEEE, 2015, pp. 1–8.

[4] J. Marck, A. Mohamoud, E. v.d. Houwen, and R. van Heijster, "Indoor radar SLAM a radar application for vision and GPS denied environments," in *2013 European Radar Conf. (EuRAD)*, 2013, pp. 471–474.

[5] C. Schönauer, E. Vonach, G. Gerstweiler, and H. Kaufmann, "3D building reconstruction and thermal mapping in fire brigade operations," in *Proc. 4th Augmented Human Int. Conf.* ACM, 2013, pp. 202–205.

[6] S. Clark and G. Dissanayake, "Simultaneous localisation and map building using millimetre wave radar to extract natural features," in *Proc. 1999 IEEE Int. Conf. Robotics and Automation*, vol. 2, 1999, pp. 1316–1321.

[7] M. Adams and E. Jose, *Robotic navigation and mapping with radar*. Artech House, 2012.

[8] D. Vivet, P. Checchin, and R. Chapuis, "Localization and mapping using only a rotating FMCW radar sensor," *Sensors 13, no. 4*, pp. 4527–4552, 2013.

[9] M. Lange and J. Detlefsen, "94 GHz 3D-imaging radar for sensor-based locomotion," in *IEEE MTT-S International Microwave Symposium Digest*, vol. 3, 1989, pp. 1091–1094.

[10] Q. Zhang and R. Pless, "Extrinsic calibration of a camera and laser range finder (improves camera calibration)," in *Proc. IEEE/RSJ Int. Conf. Intelligent Robots and Systems*, vol. 3. IEEE, 2004, pp. 2301–2306.

[11] G. Pandey, J. McBride, S. Savarese, and R. Eustice, "Extrinsic calibration of a 3D laser scanner and an omnidirectional camera," *Proc. 7th IFAC Symp. Intelligent Autonomous Vehicles*, vol. 43, no. 16, pp. 336 – 341, 2010.

[12] X. Gong, Y. Lin, and J. Liu, "3D LIDAR-camera extrinsic calibration using an arbitrary trihedron," *Sensors*, vol. 13, no. 2, pp. 1902–1918, 2013.

[13] M. I. Alba, L. Barazzetti, M. Scaioni, E. Rosina, and M. Previtali, "Mapping infrared data on terrestrial laser scanning 3D models of buildings," *Remote Sensing*, vol. 3, no. 9, pp. 1847–1870, 2011.

[14] D. Borrmann, J. Elseberg, and A. Nüchter, "Thermal 3D mapping of building façades," in *Intelligent Autonomous Systems 12*, 1st ed., ser. Advances in Intelligent Systems and Computing, S. Lee, H. Cho, K.-J. Yoon, and J. Lee, Eds. Berlin et al.: Springer, 2013, no. 193, pp. 173–182.

[15] S. Vidas, P. Moghadam, and M. Bosse, "3D thermal mapping of building interiors using an RGB-D and thermal camera," in *Proc. IEEE Int. Conf. Robotics and Automation*. IEEE, 2013, pp. 2311–2318.

[16] P. Fritsche, S. Kueppers, G. Briese, and B. Wagner, "Radar and LiDAR sensorfusion in low visibility environments," in *Proc. 13th Int. Conf. Informatics, Automation and Robotics*, vol. 2. Scitepress, 2016, pp. 30–36.

[17] O. Wulf, K. O. Arras, H. I. Christensen, and B. Wagner, "2D mapping of cluttered indoor environments by means of 3D perception," in *Proc. Int. Conf. Robotics and Automation*, vol. 4, 2004, pp. 4204–4209.

[18] P. Fritsche and B. Wagner, "Modeling structure and aerosol concentration with fused radar and LiDAR data in environments with changing visibility," in *IEEE/RSJ Int.Conf. Intelligent Robots and Systems*, 2017, in Press.

[19] B. Zeise and B. Wagner, "Temperature correction and reflection removal in thermal images using 3D temperature mapping," in *Proc. 13th Int. Conf. Informatics in Control, Automation and Robotics*, vol. 2. Scitepress, 2016, pp. 158–165.